Molecular Adsorption to LiMo$_3$Se$_3$ Nanowire Film Chemiresistors

Xiubin Qi,[†] Frank E. Osterloh,*,[†] S. A. Barriga,[‡,§] J. A. Giacomo,[‡] and S. Chiang*,[‡]

Department of Chemistry and Department of Physics, University of California, 1 Shields Avenue, Davis, California 95616

Thin films of metallic nanowire bundles derived from the Chevrel compound LiMo$_3$Se$_3$ undergo reversible increases of their electrical resistance (up to 70%) upon exposure to vapors of organic solvents (Qi, X. B.; Osterloh, F. E. *J. Am. Chem. Soc.* 2005, *127* (21), 7666−7667). Using quartz crystal microbalance measurements with four analytes, we demonstrate here that the temporal and steady-state resistance changes of the films depend on the time following the adsorption and on the number of molecules that adsorb to the nanowire films at a given pressure. The adsorption ability of the films and the corresponding film resistance increase in the row: hexane < THF < ethanol < DMSO, closely following the polarities of the solvents. On average, ~10^5 analyte molecules per LiMo$_3$Se$_3$ unit are required to produce a measurable electrical response. Atomic force microscopy scans on nanowire films reveal that analytes deposit on top of the nanowire bundles and cause the films to swell by ~6% in volume. The temporal and steady-state resistance data of the LiMo$_3$Se$_3$ chemiresistors can be explained by assuming that coating of the nanowire bundles with analyte molecules reduces the interwire charge transport in the films.

Great interest surrounds function and applications of nanowire (NW)-based sensors, eight types of which (based on silicon,[1] carbon nanotubes,[2] palladium metal,[3] SnO$_2$,[4] Au,[5,6] ZnO,[7,8] TiO$_2$[9,10]

and polyaniline[11]) are presently known. These devices rely on changes of the conductivity of metallic and semiconducting NWs caused by analyte adsorption onto the NW surface or analyte dissolution in the NW material. Several mechanisms have been proposed to explain these effects.[12] In the case of carbon nanotubes,[2,13] ZnO nanowires, and polyaniline nanofibers,[11] the mechanism is believed to involve an analyte-induced doping of the NWs resulting in a change of the charge carrier concentration. For silicon NWs, the effect originates from analyte-induced gating,[1] whereas metallic Pd NWs swell in the presence of hydrogen gas, which causes the concentration of break junctions in the NW to diminish.[3]

We recently showed that thin films of metallic LiMo$_3$Se$_3$ nanowires (Figure 1) also respond to gaseous chemical analytes with reversible changes of their electrical resistance.[14] LiMo$_3$Se$_3$ nanowires consist of stacked triangular Mo$_3$Se$_3$$^-$ units whose negative charge is compensated by lithium ions that are electrostatically associated with the nanowires.[15,16] The chemielectrical properties of LiMo$_3$Se$_3$ films are of potential interest for the construction of chemical sensors,[17] but the origin of the resistance changes in these films and the details of the molecular adsorption to the nanowires are still not known.

To better understand the mechanism of these sensors and to optimize their properties, we have carried out quartz crystal microbalance (QCM) measurements of the temporal and pressure-dependent molecular adsorption to the films. The data for four different molecular analytes reveal that the analyte adsorption to the film is correlated with the electrical property changes in the time and in the analyte pressure domain. Using atomic force microscopy (AFM) scans, we also find that the adsorption of the analytes causes the thickness of individual nanowire bundles and, in particular, of nanowire junctions to increase. Tentatively, we identify the deposition of analyte molecules between nanowire bundles and the corresponding formation of break junctions as the cause for the increase of the electrical resistance of these films.

* Corresponding author. E-mail: fosterloh@ucdavis.edu. Fax: (530) 752-8995.
† Department of Chemistry.
‡ Department of Physics.
§ Current address: Department of Physics, University of California, Berkeley, CA 94720.

(1) Cui, Y.; Wei, Q. Q.; Park, H. K.; Lieber, C. M. *Science* **2001**, *293* (5533), 1289−1292.
(2) Kong, J.; Chapline, M. G.; Dai, H. J. *Adv. Mater.* **2001**, *13* (18), 1384−1386.
(3) Favier, F.; Walter, E. C.; Zach, M. P.; Benter, T.; Penner, R. M. *Science* **2001**, *293* (5538), 2227−2231.
(4) Wang, Y. L.; Jiang, X. C.; Xia, Y. N. *J. Am. Chem. Soc.* **2003**, *125* (52), 16176−16177.
(5) Li, C. Z.; He, H. X.; Bogozi, A.; Bunch, J. S.; Tao, N. J. *Appl. Phys. Lett.* **2000**, *76* (10), 1333−1335.
(6) Bogozi, A.; Lam, O.; He, H. X.; Li, C. Z.; Tao, N. J.; Nagahara, L. A.; Amlani, I.; Tsui, R. *J. Am. Chem. Soc.* **2001**, *123* (19), 4585−4590.
(7) Kind, H.; Yan, H. Q.; Messer, B.; Law, M.; Yang, P. D. *Adv. Mater.* **2002**, *14* (2), 158−+.
(8) Wang, Z. L. *Adv. Mater.* **2003**, *15* (5), 432−436.
(9) Iwanaga, T.; Hyodo, T.; Shimizu, Y.; Egashira, M. *Sens. Actuators, B: Chem.* **2003**, *93* (1−3), 519−525.
(10) Varghese, O. K.; Gong, D. W.; Paulose, M.; Ong, K. G.; Grimes, C. A. *Sens. Actuators, B: Chem.* **2003**, *93* (1−3), 338−344.
(11) Huang, J.; Virji, S.; Weiller, B.; Kaner, R. *J. Am. Chem. Soc.* **2003**, *125* (2), 314−315.
(12) Kolmakov, A.; Moskovits, M. *Annu. Rev. Mater. Res.* **2004**, *34*, 151−180.
(13) Kong, J.; Franklin, N. R.; Zhou, C. W.; Chapline, M. G.; Peng, S.; Cho, K. J.; Dai, H. J. *Science* **2000**, *287* (5453), 622−625.
(14) Qi, X. B.; Osterloh, F. E. *J. Am. Chem. Soc.* **2005**, *127* (21), 7666−7667.
(15) Tarascon, J. M.; DiSalvo, F. J.; Chen, C. H.; Carroll, P. J.; Walsh, M.; Rupp, L. *J. Solid State Chem.* **1984**, *58*, 290−300.
(16) Potel, M.; Chevrel, R.; Sergent, M.; Armici, J. C.; Decroux, M.; Fischer, O. *J. Solid State Chem.* **1986**, *35*, 286−290.
(17) Albert, K.; Lewis, N.; Schauer, C.; Sotzing, G.; Stitzel, S.; Vaid, T.; Walt, D. *Chem. Rev.* **2000**, *100* (7), 2595−2626.
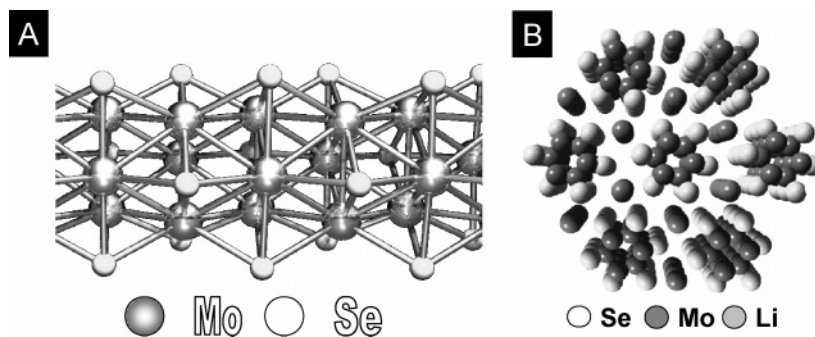
Figure 1. (A) Schematic drawing of a fragment of a single $LiMo_3Se_3$ strand (Li^+ omitted). (B) Cross section of nanowire bundle.

EXPERIMENTAL SECTION

All preparations and conductivity measurements were carried out in a nitrogen glovebox (O_2 level <10 ppm) unless stated otherwise, using degassed solvents of reagent grade dimethyl sulfoxide (DMSO) 99.7%, tetrahydrofuran (THF) 99.9%, ethanol 99.9%, methanol 99.9%, and hexane 99.9%). Nanowire dispersions in DMSO were obtained by exfoliation of the Chevrel phase $LiMo_3Se_3$[18] as described earlier.[19] The electrode arrays were homemade using standard lithographic procedures. The arrays were composed of several fingers of 100-nm-thick indium tin oxide films on borosilicate glass. The fingers were 2 cm long and 1.27 mm wide, with a spacing of 0.50 mm.

Nanowire Films. Nanowire films were obtained by depositing one drop of concentrated $LiMo_3Se_3$ solution (2.44 mM) in DMSO onto quartz crystals for adsorption measurements or onto lithographically patterned glass slides on top of two electrode fingers for conductivity measurements. After removal of the solvent in a vacuum, the thickness of the films was determined with atomic force microscopy (tapping mode).

Conductivity Measurements. Electrode arrays containing the nanowire films were mounted in a sealed chamber (~20 mL) at 25 °C under vacuum (10 mTorr). A volume of 0.2 mL of saturated analyte vapor (in nitrogen) was injected with a syringe into the chamber, and the resistance was followed with a PC-controlled Keithley 7200 multimeter. After 1 min, another 0.2 mL of the vapor was injected. The above procedure was repeated until a total of 1 mL of vapor had been injected. For time-dependent measurements, a single volume of 1.0 mL of saturated analyte vapor (hexane, THF, ethanol, and DMSO) was injected into the chamber, and the conductivity was monitored.

QCM Measurements. A XTM/2 deposition monitor (Leybold) and a quartz crystal sensor (Maxtek) were employed for the microgravimetric analysis of the adsorption of analyte molecules on a $LiMo_3Se_3$ film. A quartz crystal (2.0 × 2.0 mm) coated with a 60-nm-thick nanowire film (mass ~5.1 µg) was mounted onto the electrode in a homemade sealed chamber (~500 mL). The chamber was evacuated (20 mTorr) and kept at 25 °C. For each measurement, 5 mL of saturated analyte vapor (hexane, THF, ethanol, or DMSO) was then injected into the chamber, and the mass increase was recorded. After stabilization, another 5 mL of vapor was injected. This was repeated until a total of 25 mL of

vapor had been injected. For time-dependent measurements, a single volume of 20 mL of saturated analyte vapor (hexane, THF, ethanol, or DMSO) was injected into the chamber, and the mass increase was recorded.

Other Measurements. Scanning electron (SEM) and transmission electron (TEM) micrographs were recorded on a FEI XL30-SFEG and a Philips CM12, respectively. Samples were prepared using holey carbon-coated TEM grids (TedPella) or patterned indium tin oxide (ITO)-coated glass slides as supports. AFM measurements were performed on a Digital Instruments Nanoscope III Multimode AFM in tapping mode using Si probes (150 kHz, 5 N m). To evaluate the swelling of the film, samples were flushed with saturated vapors of methanol or DMSO in nitrogen immediately before the measurement.

RESULTS AND DISCUSSION

Films of exfoliated $LiMo_3Se_3$ nanowires were prepared by casting a measured amount of the nanowire dispersion in DMSO onto a ITO microelectrode substrate and by removing the solvent in a vacuum. This produces 5−100-nm-thick films of randomly oriented nanowire bundles (inset in Figure 2A). TEM images (Figure 2A) reveal that bundles deposited from a 2.44 mM nanowire solution in DMSO are 6 ± 4 nm thick, which corresponds to ~37 individual strands, assuming hexagonal close packing. The lengths of the nanowires are determined by the dimensions of the $InMo_3Se_3$ crystals, from which $LiMo_3Se_3$ is obtained by isomorphous cation exchange. These crystals are 10−15 µm long (see SEM image in Figure S-1, Supporting Information).

After deposition of the nanowires onto flat-band electrodes, it is possible to monitor the lateral film conductance and to employ the films as chemical sensors (for design of the chemiresistor see, Qi and Osterloh[14]). Upon exposure to 4.14 Torr ethanol vapor (in N_2), the lateral conductivity of a ~60-nm-thick film changes as shown in Figure 2B. The resistance increases within milliseconds after addition of the analyte vapor and then slowly reaches its maximum value after ~10 s. The resistance increase and the response time are determined by the thickness of the films, by the partial pressure of the analytes, and by the length of the charge transport path through the film as described previously.[14] When the analyte is pumped out of the chamber, the resistance returns to the baseline following a similar asymptotic trend.

In separate resistivity and quartz crystal microbalance measurements, we determined how the observed resistance changes

(18) Tarascon, J. M.; Hull, G. W.; DiSalvo, F. J. *Mater. Res. Bull.* **1984**, *19*, 915−924.

(19) Osterloh, F. E.; Martino, J. S.; Hiramatsu, H.; Hewitt, D. P. *Nano Lett.* **2003**, *3* (2), 125−129.
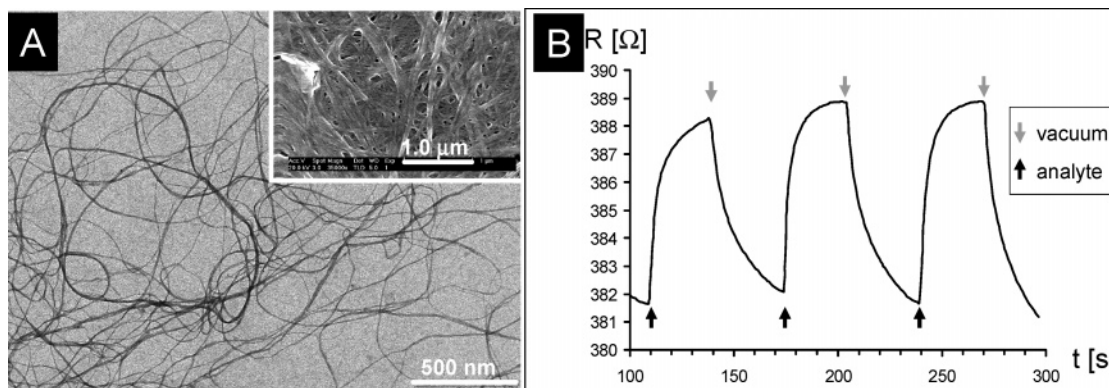
Figure 2. (A) TEM and SEM (inset) images of LiMo₃Se₃ nanowires deposited from a 2.44 mM dispersion in DMSO. (B) Analyte-induced resistance changes of a 60-nm-thick nanowire film. Addition and removal of the analyte (methanol) are indicated by arrows.
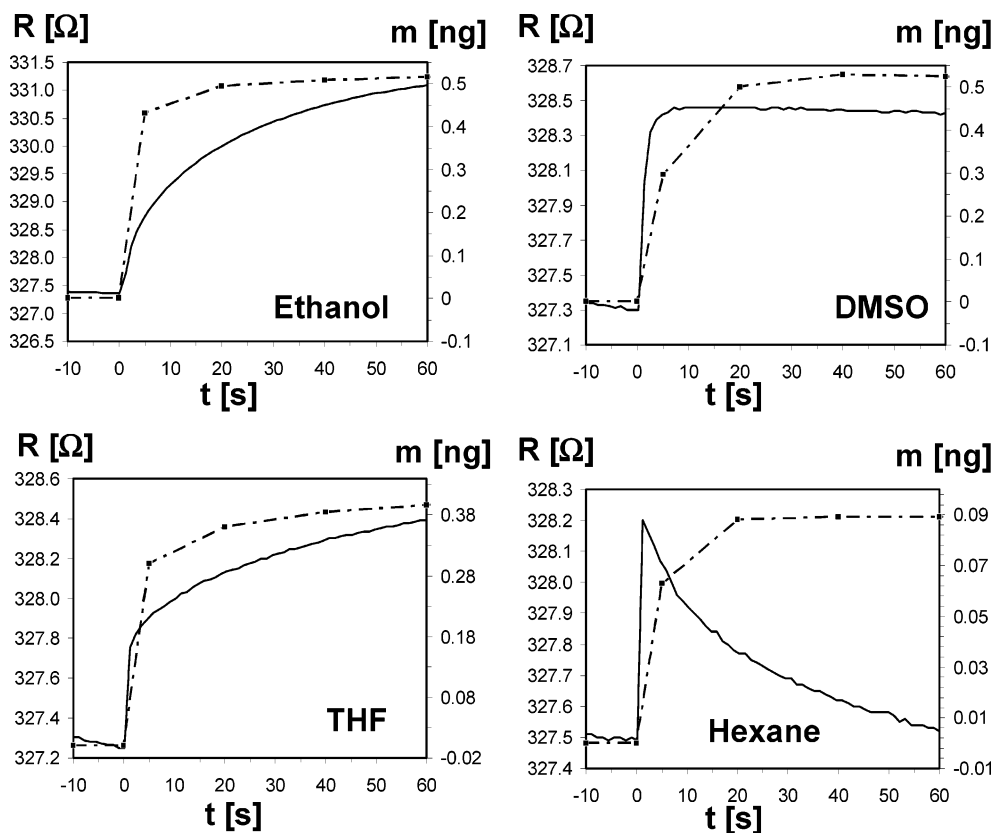

Figure 3. Time-dependent resistance (solid lines, left axes) and mass changes (broken lines, right axes) of ∼60-nm-thick nanowire films exposed to the respective analytes (partial pressures given in Table 1).

of the film are correlated with analyte adsorption. Figure 3 shows the temporal mass increase and resistance data measured on ∼60-nm-thick films. Additional data are summarized in Table 1. It can be seen that, for ethanol, DMSO, THF, and hexane, 90% of the adsorption takes place within the first ∼20 s of injection. Saturation is reached after ∼40 s, except for hexane, which saturates within ∼20 s.

The electrical resistance increase of the films roughly follows the mass increase, except for hexane, where the resistance increases only in the first second after analyte injection and then drops quickly almost to the baseline. The resistance pattern in this case indicates a complex relationship between adsorption and resistance. Interestingly, for both THF and ethanol, resistance increases are slower than the mass increases. Ninety percent of the final resistance is reached after ∼40 s, i.e., twice the time it

takes the analytes to adsorb to the film. On the contrary, for DMSO and hexane, the resistance increases faster than the analyte adsorption, and 90% of the maximum resistance is reached after less than 3 and 1 s, respectively, for these analytes.

The different detection time scales cannot be explained solely on the basis of analyte mobility in the films. The detection times increase in the order hexane < DMSO < THF ≈ ethanol, whereas the viscosity coefficients of the analytes increase in the order, hexane (0.0029)[20] < THF (0.0045)[21] < ethanol (0.012)[20] < DMSO (0.0198)[22] (all values as g cm⁻¹ s⁻¹ at 25 °C). This suggests that besides analyte adsorption and analyte distribution, at least one

(20) Weast, R. C., Ed. *CRC Handbook of Chemistry and Physics*, 1st student ed.; CRC Press: Boca Raton, FL, 1988.
(21) Ottani, S.; Vitalini, D.; Comelli, F.; Castellari, C. *J. Chem. Eng. Data* **2002**, *47* (5), 1197−1204.

Table 1. Temporal Mass Changes and Resistance Response Times for ~60-nm LiMo₃Se₃ Nanowire Films (0.08 cm²)

	THF (7.6 Torr)	hexane (7.6 Torr)	ethanol (4.1 Torr)	DMSO (0.04 Torr)
total electrical change (Ω)	1.14	0.03	3.73	1.13
electrical response time (s)[a]	>39	<1	>39	<3
total mass change (ng)	0.40	0.09	0.52	0.52
molar ratio of analyte vs LiMo₃Se₃	5.8×10^5	1.1×10^5	1.2×10^6	7.0×10^5
mass response time (s)[a]	<20	<20	<20	<20

[a] When 90% of change has occurred.

additional process is involved in generating resistance changes in the chemiresistors.

Steady-state mass and resistance increases for a ~60-nm-thick nanowire film are shown in Figure 4A and B. The respective values were obtained 1 min after injection, when the reading had stabilized. It can be seen that, in the pressure interval that was investigated, the analyte adsorbate mass is linearly dependent on the analyte partial pressure, regardless of analyte. The slopes of the adsorbate−pressure curves differ significantly among the analytes and can be taken as a measure of the binding affinity of the analyte to the films. The binding affinity to the film increases in the row, hexane < THF < ethanol < DMSO. This trend seems to be correlated with the polarity of the solvents, which increases in the same order (hexane, 1.89[20] < THF, 7.36[23] < ethanol, 24.3[20] < DMSO, 46.1;[24] values as dimensionless dielectric constants at 25 °C). This makes sense if one considers that the ionic compound Li⁺Mo₃Se₃⁻ would favor a polar environment. The enhanced uptake of those analytes also explains the slower film adsorption kinetics in comparison to hexane (see discussion above). Due to their strong binding ability, DMSO, ethanol, and THF can diffuse deep into the nanowire film, whereas hexane adsorption is restricted to the film surface.

The steady-state resistance curves in Figure 4B closely resemble the mass increase plots. All resistance increases are also linear, and the relative effects of the analytes on the resistance of the films follow the same trend as observed for the mass increases. A direct comparison of adsorption and resistance is shown in Figure 4C, where the relative molar binding affinities (derived from the slopes of plots in 4B) of the four analytes are plotted together with respective changes of the electrical resistance of the film. The two parameters match well for all analytes, except for hexane, whose induced resistance change is 1 order of magnitude smaller than expected. This discrepancy suggests that the physical processes in the film following the adsorption of hexane are different from those induced by DMSO, ethanol, and THF.

To obtain additional information about the processes in the films associated with the adsorption of analytes, AFM profile scans were recorded on nanowire films prior to and during the application of saturated solvent vapors in a nitrogen atmosphere. Scans obtained for a 27 ± 7 nm multilayer film before (left) and after the addition of methanol vapor (right) are shown in Figure

5A. Overall, the images for the dry and wet film are very similar, except for a slight increase of the apparent film density in the right image. The height scans in Figure 5B reveal that the application of the analyte leads to an increase of the film thickness by 1.5 ± 0.7 nm. This corresponds to 6% of the original film thickness. This swelling effect is not entirely homogeneous throughout the film as can be seen from the plot in Figure 5C, which shows the film expansion as a function of the original film thickness. This effect could be caused by inhomogeneities of the film or of the analyte penetration through the film.

To identify the causes for the swelling, additional AFM scans were conducted on a nanowire monolayer (Figure 5D) before and after treatment with saturated DMSO vapor (in N₂). Height data of individual bundles and of nanowire junctions is summarized in Figure 5E and F. The data clearly show that analyte adsorption leads to an increase in bundle diameter by on average 0.12 nm (2.5% of their thickness). This increase, however, is nearly the same for bundles of different thicknesses, suggesting that it is not due to a swelling of the bundles but due instead to the deposition of analyte onto their surfaces. For nanowire junctions, the overall height increase of the junctions (mean 0.7 nm, i.e., 13% of initial thickness) is ~4 times stronger on a percentage basis than that of the bundles. Again, the increase in thickness does not depend on the initial thickness of the junctions, ruling out a swelling of the bundles, and suggesting condensation of analytes. The condensation is also directly visible in the AFM scan in the highlighted circles in Figure 5D, where solvent droplets begin to appear around the junctions. A preferential adsorption of analytes between crossed nanowire bundles is likely to be due to the capillary forces resulting from the enhanced surface area at these positions.

The findings from the AFM and QCM study suggest that the chemiresistive properties of LiMo₃Se₃ nanowire films can be explained in terms of a "break junction model" similar to that described by Penner et al.[3] Break junctions are structure defects with limited or no conductivity. In our case, analyte condensation on the nanowire bundles leads to an increase of the bundle separation causing similar break junctions to appear in the film and leading to an overall increase of the film resistance. This model agrees with the principal findings of this study, namely, that relatively large amounts of analytes are required to produce a resistance change (~10⁵ molecules per LiMo₃Se₃; for details, see Table 1) and that the sensitivity of the films depends on the polarity of the analytes (i.e., polar analytes form better films on the polar nanowire bundes). Based on this model, the structural reorganization of the film (swelling) and analyte diffusion through

(22) Aralaguppi, M. I.; Aminabhavi, T. M.; Harogoppad, S. B.; Balundgi, R. H. *J. Chem. Eng. Data* **1992**, *37*, 298−303.

(23) Anno, N.; Delisi, R.; Goffredi, M.; Liveri, V. T. *J. Chem. Soc., Faraday Trans.* **1982**, *78*, 3101−3108.

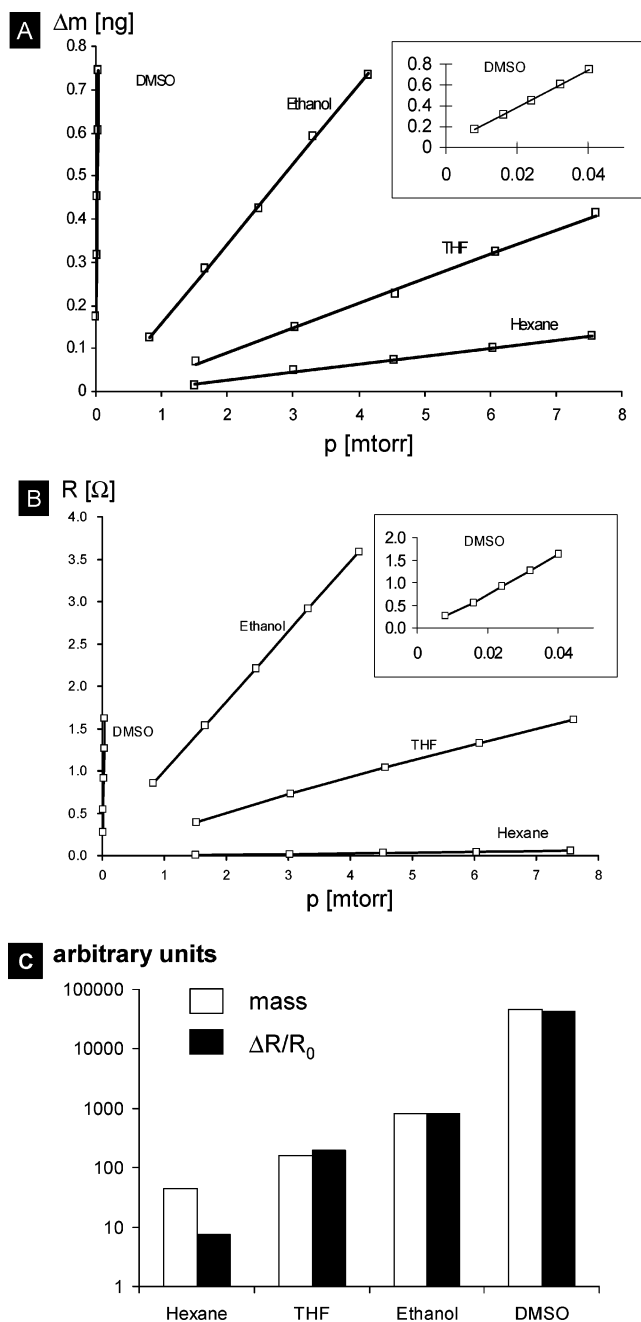(24) Ritzoulis, G. *Can. J. Chem.* **1989**, *67*, 1105−1108.

Figure 4. (A) Steady-state mass and (B) resistance changes of ~60-nm-thick nanowire films exposed to the DMSO, hexane, THF, and ethanol at the indicated partial pressures. The data for DMSO are also shown in the insets. (C) Histogram comparing molar amounts of adsorbed analytes (at equal partial pressure) and steady-state resistance changes (DMSO, dimethyl sulfoxide; THF, tetrahydrofuran).
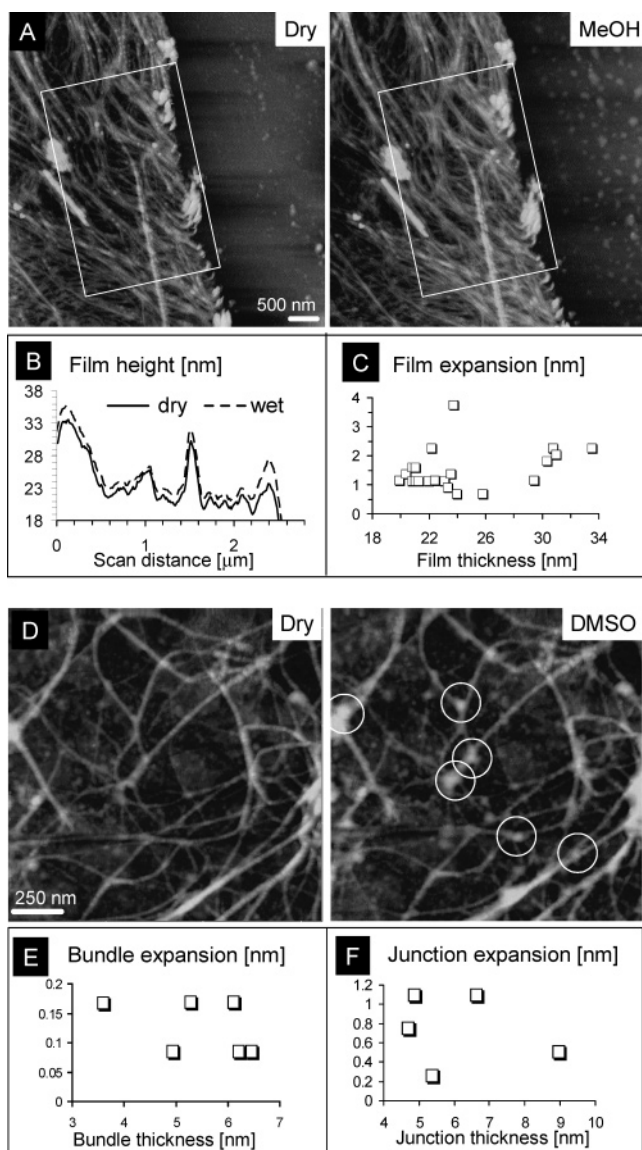

Figure 5. Morphology changes in nanowire multilayer and single-layer films on silicon. (A) Multilayer film before and after adsorption of methanol (note methanol droplets on glass substrate in right image). For height measurements, the film was scratched with the tip of a pair of tweezers. Needlelike objects correspond to incompletely exfoliated $LiMo_3Se_3$. The white frame denotes the area used for the section analysis in (B). (B) Film profile scans before and after treatment with analyte. Two average profiles were obtained by averaging multiple scans along the shorter side of the area shown in (A). (C) Film expansion versus original film thickness. (D) Nanowire monolayer on glass before (left) and after application of DMSO vapor (right). Circles denote formation of DMSO droplets. (E) Plots of nanowire bundle expansion and nanowire junction expansion (F).

the film are the principal causes for the observed delay times between analyte adsorption and resistance change.

CONCLUSIONS

The present investigation demonstrates that the resistance changes in $LiMo_3Se_3$ nanowire films are directly related to the quantitative molecular adsorption of DMSO, THF, ethanol, and hexane. Time-dependent measurements reveal adsorption times on the order of 20 s or less, with the electrical response time increasing in the order, hexane < DMSO < THF ≈ ethanol.

Analyte pressure-dependent measurements show that the binding affinity increases in the order, hexane < THF < ethanol < DMSO, i.e., with increasing analyte polarity. The observed steady-state resistance changes closely follow the molecular adsorption, suggesting that both processes are correlated with each other. AFM profile scans on multilayered nanowire films demonstrate that methanol causes a swelling of the films by 6% and that DMSO vapor condenses on the surface of nanowire bundles and between nanowire junctions. The chemiresistive properties of the $LiMo_3$-

Se_3 films are explained in terms of the formation of break junctions as described above. Further studies on utilizing the chemically dependent electrical properties of $LiMo_3Se_3$ nanowire films for the preparation of selective sensors are underway.

SUPPORTING INFORMATION AVAILABLE

Scanning electron micrograph of $InMo_3Se_3$. This material is available free of charge via the Internet at http://pubs.acs.org.